

$^{176}\text{Lu}^+$ clock comparison at the 10^{-18} level via correlation spectroscopy

Zhang Zhiqiang,¹ K. J. Arnold,^{1,2} R. Kaewuam,¹ and M. D. Barrett^{1,3,4,*}

¹Centre for Quantum Technologies, 3 Science Drive 2, 117543 Singapore

²Temasek Laboratories, National University of Singapore, 5A Engineering Drive 1, 117411 Singapore

³Department of Physics, National University of Singapore, 2 Science Drive 3, 117551 Singapore

⁴National Metrology Centre, Agency for Science, Technology and Research (A*STAR), 8 CleanTech Loop, Singapore 637145

We experimentally demonstrate agreement between two $^{176}\text{Lu}^+$ frequency references using correlation spectroscopy. From a comparison at different magnetic fields, we obtain a quadratic Zeeman coefficient of $-4.89264(88)$ Hz/mT², which gives a corresponding fractional frequency uncertainty contribution of just 2.5×10^{-20} for comparisons at typical operating fields of 0.1 mT. A subsequent comparison with both systems at 0.1 mT, demonstrates a fractional frequency difference of $(-2.0 \pm (3.7)_{\text{stat}} \pm (0.9)_{\text{sys}}) \times 10^{-18}$, where ‘stat’ and ‘sys’ indicate statistical and systematic uncertainty, respectively.

The last two decades has seen rapid development of optical atomic clocks, with many systems now reporting fractional performance at the 10^{-18} level [1–7]. Such performance has many important applications, such as defining the geoid [8], monitoring geopotential changes [9], measuring time and frequency [10], and testing fundamental physics [11]. Independent of the proposed application, it is important to explore a wide range of atomic systems to assess their merits and long-term potential for future development. In this work we demonstrate the ease at which two $^{176}\text{Lu}^+$ references can achieve agreement at $\lesssim 10^{-18}$. From a comparison at different magnetic fields, we obtain a quadratic Zeeman coefficient of $-4.89264(88)$ Hz/mT², which gives a corresponding fractional frequency uncertainty contribution of just 2.5×10^{-20} for comparisons at typical operating fields of 0.1 mT. A subsequent comparison with both systems at 0.1 mT, demonstrates a fractional frequency difference of $(-2.0 \pm (3.7)_{\text{stat}} \pm (0.9)_{\text{sys}}) \times 10^{-18}$, where ‘stat’ and ‘sys’ indicate statistical and systematic uncertainty, respectively. Due to the clock transition’s insensitivity to external electromagnetic perturbations, results were obtained without magnetic shielding [12] or active field stabilization, without ground state cooling using simulations to justify its effectiveness [13], without extreme temperature measurement and control [1–3, 14], or even the use of simulations and thermal cameras for a more moderate temperature assessment [4, 15]. Such ease of use offers considerable technical advantages for practical implementations of an atomic frequency reference.

Singly ionized lutetium is a two electron system with three available clock transitions and the relevant level structure is shown in Fig. 1a. As described in previous work [16, 17], laser beams at 350, 622, and 895 nm facilitate optical pumping into the long-lived 3D_1 state, laser beams at 646 nm facilitate detection, Doppler cooling, and state preparation of $|7\rangle \equiv |^3D_1, 7, 0\rangle$, and microwaves are used to drive transitions between the 3D_1 hyperfine states. This work concerns the $^1S_0 \leftrightarrow ^3D_1$ transition at 848 nm, which has favourable properties as

a frequency reference. The blackbody radiation (BBR) shift is $\approx -1.36(10) \times 10^{-18}$ at 300 K [18, 19], which is sufficiently small that any temperature-induced frequency difference between two references operating within a temperature range of $25 \sim 60^\circ\text{C}$ is $\lesssim 10^{-18}$. At a typical operating magnetic field of 0.1 mT, transitions between the $m = 0$ states have the lowest sensitivity to magnetic field noise of any existing clock system, being at least five-fold smaller than those in neutral lattice clocks [1, 3], a 100-fold smaller than in Al^+ [20], and five orders of magnitude smaller than those in the alkaline-earth ions (Ca^+ and Sr^+)[12, 21]. The large atomic mass makes it less susceptible to motional shifts than lighter ions and the secondary clock transition at 804 nm provides exceptional detectability of micromotion. Owing to the upper-state lifetime of approximately one week, the dominant systematic is the probe-induced ac Stark shift, which is 200-fold smaller than for the Yb^+ E3 clock transition under the same interrogation conditions [18, 19, 22].

All clock systems use some form of averaging, which is typically an averaging over one or more pairs of Zeeman lines [23] or over orientations of the magnetic field [24]. In the case of $^{176}\text{Lu}^+$, we use an averaging over transitions from $|g\rangle \equiv |^1S_0, 7, 0\rangle$ to the hyperfine states $|F\rangle \equiv |^3D_1, F, 0\rangle$ where $F = 6, 7$, and 8 [25]. The average can be conveniently realized using a hybrid microwave and optical interrogation [26], which we refer to here as hyperfine-averaged Ramsey spectroscopy (HARS). As illustrated in Fig. 1b&c, the interrogation sequence consists of a Ramsey interrogation on the $|g\rangle \leftrightarrow |8\rangle$ transition and microwave transitions within the interrogation time to transfer population between the hyperfine states. Timing is such that the effective time in each of the hyperfine states is the same. When the laser is served to the central Ramsey fringe, the hyperfine-averaged (HA) clock frequency is given by

$$f = \frac{1}{3}(f_8 + f_7 + f_6) = f_L + \frac{1}{3}(2f_1 + f_2), \quad (1)$$

where f_F is the resonant frequency of the $|g\rangle \leftrightarrow |F\rangle$

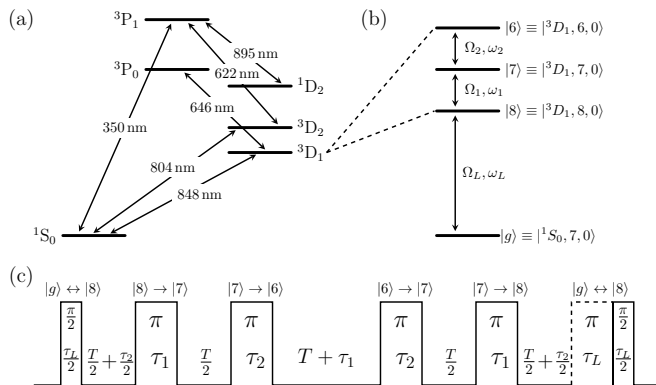


FIG. 1. $^{176}\text{Lu}^+$ spectroscopy (a) Atomic level structure of $^{176}\text{Lu}^+$ showing the wavelengths of transitions used. (b) Levels of the 848-nm clock transition used in the clock interrogation sequence. Ω_α and ω_α denote the coupling strengths and frequencies for the fields driving the transitions indicated. (c) Clock interrogation sequence for HARS. An optional π -pulse on the optical transition is included when implementing hyper-Ramsey spectroscopy to suppress probe-induced ac-Stark shifts.

transition, $f_L = \omega_L/(2\pi)$ is the laser frequency, and $f_k = \omega_k/(2\pi)$ for $k = 1, 2$ are the microwave frequencies used within the interrogation sequence. As explained in previous work [26], the interrogation sequence ensures $f_L + (2f_1 + f_2)/3$ represents the HA clock frequency, as indicated by Eq. 1, even if the microwave fields are not exactly resonant.

Comparisons were carried out on two ions held in separate traps, denoted Lu-1 and Lu-2, the details of which are reported elsewhere [17, 27]. As our laser coherence limits interrogation times to ~ 50 ms, we use correlation spectroscopy [28–30], which allows extended probe times by factoring out laser noise. In our case we have been able to extend interrogation times to over 700 ms, which is limited only by a heating problem in one trap (Lu-1). Each comparison consisted of three interleaved experiments: one to measure the frequency difference, δf , between the two atomic references using HARS; one to keep the 848-nm clock laser near to resonance with the $|g\rangle \leftrightarrow |8\rangle$ transition using Rabi spectroscopy; and one to monitor the magnetic field in each chamber using microwave spectroscopy of the $|^3D_1, 7, 0\rangle \leftrightarrow |^3D_1, 6, \pm 1\rangle$ transition. The duty cycle for measuring the frequency difference was 87% for the longest interrogation times used in the experiments.

Typical systematic effects for the comparison experiments are given in table I. The dominant systematic shift arises from the probe-induced ac-Stark shift. This was measured in each trap by interleaving Rabi and hyper-Ramsey spectroscopy [22, 31] of the $|g\rangle \leftrightarrow |8\rangle$ transition with the frequency difference determining the probe-induced ac-Stark shift, δ_k , for Lu- k . For HARS, the re-

sulting shift given in table I is [31]

$$\delta_{s,k} = \frac{\delta_k}{1 + \frac{\pi}{2} \frac{T_R}{\tau_L}}, \quad (2)$$

where $T_R = 3(T + \tau_1 + \tau_2)$ is the total interrogation time and τ_L is the π -pulse time for the clock transition. Several ac-Stark shift measurements were taken throughout the campaign and the δ_k for each experiment is determined from measurements of nearest proximity. As the shift is not continuously monitored, we assumed a 5% uncertainty in the ac-Stark for each trap to allow for possible variation during the experiment but bound by the maximum variation observed between measurements. The value of δ_k given in table I is a single representative example.

Excess micromotion (EMM) was evaluated on the $|^1S_0, 7, 0\rangle \leftrightarrow |^3D_2, 9, 0\rangle$ transition at 804 nm by the resolved sideband technique [32] and several measurements were carried out throughout the campaign. For each trap, the mean and half the difference of the largest and smallest determinations are given for the shift and uncertainty, respectively. Thermal motion was investigated from dephasing when driving the $|g\rangle \leftrightarrow |8\rangle$ transition and variable delays before probing were used to estimate heating rates. The associated second-order Doppler shift is dominated by a high heating rate in Lu-1 and the fractionally larger uncertainty arises from the accuracy at which that could be assessed. The heating rates were 2.3(0.8) mK/s and 0.099(15) mK/s for Lu-1 and Lu-2, respectively. These were measured repeatedly throughout the campaign, with the larger heating rate being measured almost daily.

Time-varying magnetic fields give rise to an ac-Zeeman shift with the dominant contributions coming from currents in the electrodes driven by the rf-trapping potential. The contribution depends on the component of the rf-magnetic field perpendicular to the applied dc field [33]. This was measured from an Autler-Townes splitting on the Ba^+ clock transition [27], giving rms values of 0.98(1) μT and 0.52(1) μT for Lu-1 and Lu-2 respectively.

The microwave fields used in HARS can also contribute to an ac-Zeeman shift [26]. Inasmuch as practically possible, microwave antennas are positioned to maximise the π component and balance the σ^\pm components, which suppresses the contribution to $\lesssim 7 \times 10^{-19}$ for any of the comparisons reported here. The microwave field components are deduced from measured π -times on the $|7, 0\rangle \leftrightarrow |F, m_F = 0, \pm 1\rangle$ where $F = 6, 8$ and the uncertainty given in the table is based on a 5% inaccuracy for the measured π -times. Detailed calculations are given in the supplemental material.

The hyperfine interaction gives rise to a quadrupole shift that is not eliminated by HA. The shift is characterized by a residual quadrupole moment of $-2.5 \times 10^{-4} e a_0^2$

TABLE I. Characteristic uncertainty budget. All values are relative to 10^{-18} of the HA frequency. The values given here are for experiment 7 for which $\tau_L = 8$ ms, $\tau_1 = \tau_2 = 24$ ms, and $T = 200$ ms with an applied static magnetic field of ≈ 0.1 mT for both traps. Tables for experiments 1 to 6 are given in the supplemental material.

Effect	Lu-1		Lu-2		Difference	
	Shift	Unc.	Shift	Unc.	Shift	Unc.
Excess micromotion	-0.41	0.37	-0.44	0.34	0.03	0.50
Second-order Doppler (thermal)	-1.87	0.45	-0.13	0.06	-1.75	0.45
ac-Zeeman (rf)	0.54	0.01	0.15	0.01	0.39	0.01
ac-Zeeman (microwave)	-0.06	0.04	-0.06	0.15	-0.01	0.16
Gravity shift ^a	-	-	-	-	-1.31	0.15
ac-Stark shift	-126.59	6.33	-125.14	6.26	-1.45	8.90
HARS timing	2.60	1.33	4.88	0.72	-2.28	1.51
Microwave coupling	0	0.21	0	0.21	0	0.30
Optical coupling	0	0.28	0	0.28	0	0.39
Residual quadruple shift	0.22	0.02	0	0.32	0.22	0.32
Total shift	-125.58	6.50	-120.74	6.33	-6.15	9.07

^a Only differential shifts are considered.

as determined from a combination of g -factor measurements and theory [16]. The shift can then be estimated using the quadrupole shift extracted from $S_{1/2} \leftrightarrow D_{5/2}$ clock measurements in Ba^+ and rescaling the quadrupole moments. This has been done for Lu-1 [27], which gives an estimated shift of 2.2×10^{-19} with a 10% uncertainty ascribed to the value of the quadrupole moment. For Lu-2, the maximum possible shift from the dc confinement would be 3.2×10^{-19} if the magnetic field was aligned along the trap axis. For both traps, the magnetic field is at an angle of approximately 57° to the trap axis. As such, we would expect a reasonable suppression of the component from the trapping potentials and the shift dominated by stray fields. As it is unlikely a shift from stray fields would exceed the maximum possible shift from the dc confinement, we bound the shift by $\pm 3.2 \times 10^{-19}$.

In the analysis of HARS [26] it was assumed the detuning of the microwaves was much smaller than the associated coupling strengths, and the finite duration of the optical pulses was neglected. For the level of precision obtained here, these assumptions should be reconsidered. A comprehensive analysis is given in the supplemental material. Most importantly, the finite duration of the optical pulse is associated with an effective time $2\tau_L/\pi$ spent in $|8\rangle$. As this was not accounted for by reducing the dwell time in $|8\rangle$, it results in an effective timing error. In addition, there is a much smaller correction that is practically independent of the optical pulse time. However, the influence of this term depends on the microwave and optical coupling strengths relative to the values determined by their respective π times. The uncertainties given in table I for the microwave and coupling errors corresponding to 1% and 2.5% uncertainty in the microwave and optical couplings, respectively.

A differential gravitational shift of $1.31(15) \times 10^{-18}$ is included to account for a height difference of 1.2(1) cm between the ions. All other shifts are expected to con-

tribute negligibly to the frequency difference compared to the statistical uncertainty achieved in the comparisons. A discussion of these omitted shifts is given in methods.

The quadratic Zeeman coefficient (α_z) of the $|^1S_0\rangle \leftrightarrow |^3D_1\rangle$ transition can be determined by

$$\alpha_z = \frac{\delta_z}{B_1^2 - B_2^2}, \quad (3)$$

where B_k is the applied static magnetic field for Lu- k and δ_z is the frequency difference between the two atomic references appropriately corrected for all other systematic shifts. The results from six measurements are given in Fig. 2 offset by the weighted mean. From all six measurements we obtain $\alpha_z = -4.89264(88)$ Hz/mT² with $\chi_\nu^2 = 1.30$ as discussed in methods. With $B_1 = 1.9$ mT and $B_2 = 0.1$ mT, the estimated uncertainty in α_z requires agreement of the two atomic references to within 9.0×10^{-18} when held at the same magnetic field. A further comparison (Expt. 7) was carried out with both systems at 0.1 mT to confirm this, which gave the result $(9.2 \pm (3.6)_{\text{stat}} \pm (9.1)_{\text{sys}}) \times 10^{-18}$ as determined by 4 separate measurements with a total integration time of 29.3h. As indicated in table I, the comparison is limited by the assessment of the probe-induced ac-Stark shift.

Probe-induced ac-Stark shifts can be heavily suppressed using hyper-Ramsey spectroscopy [31, 34, 35] and the principle also applies to correlation spectroscopy and HARS. Following the work of Yudin, et al. [22, 31], a hyper-Ramsey pulse can be included, as indicated in Fig. 1c, with the clock laser frequency shifted by the measured ac-Stark shift during the clock pulses, and the additional hyper-Ramsey π -pulse phase shifted by π with respect to the first $\pi/2$ -pulse. As shown in the supplemental, this not only suppresses the ac-Stark shift, but also eliminates the effective timing error from the finite optical π -time and the sensitivity to the optical coupling strength.

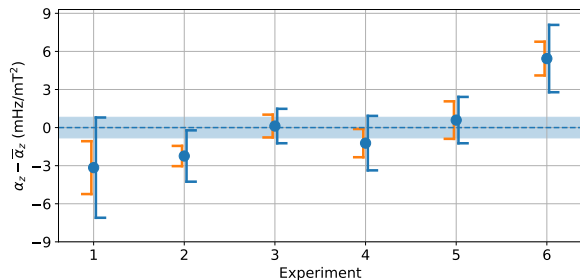


FIG. 2. Measurements of the quadratic Zeeman coefficient (α_z). Uncertainty budgets and parameters τ_L , τ_1 , τ_2 , and T and applied static magnetic fields B_1 and B_2 for each experiment are given in the supplemental. Each point is the mean of all data collected at the given parameters, corrected for systematic errors and offset by the weighted mean of all measurements. Error bars on the left represent the statistical uncertainty and those on the right are inclusive of the systematic uncertainty. The shaded region indicates the uncertainty in the weighted mean. From all six measurements we obtain the estimate $\alpha_z = -4.89264(88)$ Hz/mT², with $\chi^2_\nu = 1.30$.

A final comparison (Expt. 8) including a hyper-Ramsey pulse gave $(-2.0 \pm (3.7)_{\text{stat}} \pm (0.9)_{\text{sys}}) \times 10^{-18}$ as determined by ten measurements with a total integration time of 42.4 h. Data is shown in Fig. 3 and an error budget given in table II. With suppression of the probe-induced ac-Stark shift, the only shifts above 10^{-18} are the SD shift and the gravitational shift and these are still less than the measurement precision. Moreover, the SD shift is primarily due to a heating problem in one trap. Consequently, clock agreement at this level is not reliant on substantial corrections and control of large systematics as it is for all other clock comparisons that have been made thus far.

In summary, we have used correlation spectroscopy to compare two $^{176}\text{Lu}^+$ atomic references with an inaccuracy at the low 10^{-18} level. This has provided a high accuracy assessment of the quadratic Zeeman shift, which is the leading systematic for the $^{176}\text{Lu}^+ 1S_0 \leftrightarrow 3D_1$ clock transition. Hyper-Ramsey spectroscopy is also compatible with HARS and practically eliminates the probe-induced ac-Stark shift as the next leading systematic. This then provides a frequency reference with systematics that are easily controlled to an inaccuracy below 10^{-18} without the technical challenges faced by other systems.

An accuracy claim for an individual system would require an assessment of the blackbody radiation (BBR) shift. Presumably the use of simulations and thermal cameras [4, 15] could equally be used here, although it is unclear how to quantify such an assessment. A crude analysis as given in the methods would bound the temperature to 35(10)°C, which, due to the low BBR shift for the $1S_0 \leftrightarrow 3D_1$ transition, corresponds to an BBR shift of just $-1.56(27) \times 10^{-18}$ and gives a total uncertainty for both systems of $< 8 \times 10^{-19}$. However, although it

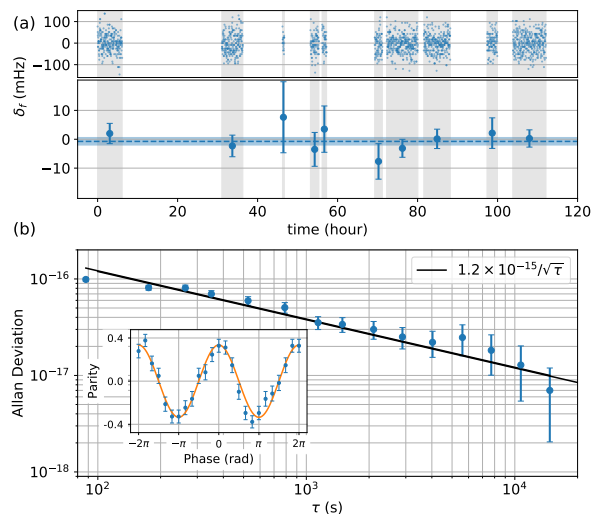


FIG. 3. **Measurement instability.** Comparison data between two $^{176}\text{Lu}^+$ references implemented via HARS including hyper-Ramsey for ac-Stark shift suppression (Expt. 8). (a) The frequency difference measured over 42.4 hours in ten runs of the experiment. Points are the mean of each run and error bars are the statistical error determined by the projection noise limit. The dashed horizontal line is the weighted mean ($\chi^2_\nu = 0.45$) and the shaded region the corresponding uncertainty, which represents a fractional frequency difference of $(-2.0 \pm (3.7)_{\text{stat}} \pm (0.9)_{\text{sys}}) \times 10^{-18}$. (b) Fractional Allan deviation for the longest single run. The inset shows a typical parity signal as a function of the relative phase of the second $\pi/2$ -pulse, the amplitude of which is limited by heating in Lu-1.

is done elsewhere [4, 36], we refrain from making any accuracy claims without a same-species comparison to the appropriate level. Here stability limits us to the low 10^{-18} , which is primarily limited by a heating problem in Lu-1.

With the lower heating rate and real-time monitoring of EMM, systematics at the mid 10^{-19} are readily achievable. Correlation spectroscopy with a 10 s interrogation time was demonstrated in our previous work [37] albeit within the same trap. In separate chambers, uncorrelated magnetic field noise may be a limiting factor. However, at the operating field of 0.1 mT, the maximum magnetic sensitivity of the 848-nm clock states is ~ 0.4 Hz/ μT . This is two orders of magnitude smaller than Al^+ , for example, for which lifetime-limited correlation spectroscopy has been claimed [30]. Increasing the interrogation time to an anticipated 10 s would make comparisons below 10^{-18} achievable on the time scale of a few days.

The relative ease at which a comparison at this level can be achieved with this system should not be underestimated. Comparisons between clock systems claiming this level of accuracy [38, 39] have variations of the measured ratios that cannot be explained by the error budgets of the individual systems, which is compelling evidence that

TABLE II. Uncertainty budget for comparison using Hyper-Ramsey (Experiment 8) for which $\tau_L = 8$ ms, $\tau_1 = \tau_2 = 24$ ms, and $T = 200$ ms with an applied static magnetic field of ≈ 0.1 mT for both traps. All values are relative to 10^{-18} of the HA frequency.

Effect	Lu-1		Lu-2		Difference	
	Shift	Unc.	Shift	Unc.	Shift	Unc.
Excess micromotion	-0.41	0.37	-0.44	0.34	0.03	0.50
Second-order Doppler (thermal)	-1.87	0.45	-0.13	0.06	-1.75	0.45
ac-Zeeman (rf)	0.54	0.01	0.15	0.01	0.39	0.01
ac-Zeeman (microwave)	-0.06	0.03	-0.13	0.11	0.07	0.11
Gravity shift ^a	-	-	-	-	-1.31	0.15
Microwave coupling	0	0.21	0	0.21	0	0.30
Residual quadruple shift	0.22	0.02	0	0.32	0.22	0.32
Total shift	-1.58	0.68	-0.55	0.60	-2.34	0.93

^a Only differential shifts are considered.

large systematic shifts are not being controlled to the levels claimed. Such problems are unlikely to occur for systems such as lutetium or thullium [40] for the simple fact that systematics are not large enough to cause such variations. Indeed, the total shift and any single contribution given in table II is, at most, at the level of the current measurement precision. Moreover, it is self-evident that systems having such low systematics have substantial room for improvement if current state-of-the-art technologies were employed to take advantage of this potential. This is particularly noteworthy for lutetium as the magnetic field sensitivity of the clock states are the lowest of any atomic system that we are aware of and the lifetime is practically indefinite. Consequently, interrogation times will not be limited by lutetium in any foreseeable future.

Acknowledgements

This work is supported by: the National Research Foundation, Prime Ministers Office, Singapore and the Ministry of Education, Singapore under the Research Centres of Excellence programme; and the National Research Foundation, Singapore, hosted by National University of Singapore under the Quantum Engineering Programme (Grant Award QEP-P5).

* phybmd@nus.edu.sg

- [1] T. L. Nicholson, S. L. Campbell, R. B. Hutson, G. E. Marti, B. J. Bloom, R. L. McNally, W. Zhang, M. D. Barrett, M. S. Safronova, G.F. Strouse, W. L. Tew, and J. Ye. Systematic evaluation of an atomic clock at 2×10^{-18} total uncertainty. *Nat. Commun.*, 6:6896, 2015.
- [2] Yao Huang, Baolin Zhang, Mengyan Zeng, Yanmei Hao, Huaqing Zhang, Hua Guan, Zheng Chen, Miao Wang, and Kelin Gao. A liquid nitrogen-cooled Ca^+ optical clock with systematic uncertainty of 3×10^{-18} . *Physical Review Applied*, 17(3):034041, 2022.
- [3] WF McGrew, X Zhang, RJ Fasano, SA Schäffer, K Belay, D Nicolodi, RC Brown, N Hinkley, G Milani, M Schioppo, et al. Atomic clock performance enabling geodesy below the centimetre level. *Nature*, 564(7734):87–90, 2018.
- [4] N Huntemann, C Sanner, B Lipphardt, Chr Tamm, and E Peik. Single-ion atomic clock with 3×10^{-18} systematic uncertainty. *Phys. Rev. Lett.*, 116(6):063001, 2016.
- [5] CW Chou, DB Hume, JCJ Koelemeij, David J Wineland, and T Rosenband. Frequency comparison of two high-accuracy Al^+ optical clocks. *Phys. Rev. Lett.*, 104(7):070802, 2010.
- [6] Masao Takamoto, Ichiro Ushijima, Noriaki Ohmae, Toshihiro Yahagi, Kensuke Kokado, Hisaaki Shinkai, and Hidetoshi Katori. Test of general relativity by a pair of transportable optical lattice clocks. *Nature Photonics*, 14(7):411–415, 2020.
- [7] Ichiro Ushijima, Masao Takamoto, Manoj Das, Takuya Ohkubo, and Hidetoshi Katori. Cryogenic optical lattice clocks. *Nature Photonics*, 9(3):185–189, 2015.
- [8] Guillaume Lion, Isabelle Panet, Peter Wolf, Christine Guerlin, Sébastien Bize, and Pacôme Delva. Determination of a high spatial resolution geopotential model using atomic clock comparisons. *Journal of Geodesy*, 91(6):597–611, 2017.
- [9] Ruxandra Bondarescu, Andreas Schäfer, Andrew Lundgren, György Hetényi, Nicolas Houlié, Philippe Jetzer, and Mihai Bondarescu. Ground-based optical atomic clocks as a tool to monitor vertical surface motion. *Geophysical Journal International*, 202(3):1770–1774, 2015.
- [10] Ian D Leroux, Nils Scharnhorst, Stephan Hannig, Johannes Kramer, Lennart Pelzer, Mariia Stepanova, and Piet O Schmidt. On-line estimation of local oscillator noise and optimisation of servo parameters in atomic clocks. *Metrologia*, 54(3):307, 2017.
- [11] MS Safronova, D Budker, D DeMille, Derek F Jackson Kimball, A Derevianko, and Charles W Clark. Search for new physics with atoms and molecules. *Reviews of Modern Physics*, 90(2):025008, 2018.
- [12] Pierre Dubé, Alan A Madej, Zichao Zhou, and John E Bernard. Evaluation of systematic shifts of the $^{88}\text{Sr}^+$ single-ion optical frequency standard at the 10^{-17} level. *Physical Review A*, 87(2):023806, 2013.
- [13] JS Chen, Samuel M Brewer, CW Chou, DJ Wineland, DR Leibrandt, and DB Hume. Sympathetic ground state cooling and time-dilation shifts in an $^{27}\text{Al}^+$ optical clock. *Phys. Rev. Lett.*, 118(5):053002, 2017.
- [14] Thomas Middelmann, Stephan Falke, Christian Lisdat, and Uwe Sterr. High accuracy correction of blackbody radiation shift in an optical lattice clock. *Phys. Rev. Lett.*,

- 109(26):263004, 2012.
- [15] Miroslav Doležal, Petr Balling, Peter BR Nisbet-Jones, Steven A King, Jonathan M Jones, Hugh A Klein, Patrick Gill, Thomas Lindvall, Anders E Wallin, Mikko Merimaa, et al. Analysis of thermal radiation in ion traps for optical frequency standards. *Metrologia*, 52(6):842, 2015.
- [16] Zhang Zhiqiang, KJ Arnold, R Kaewuam, MS Safronova, and MD Barrett. Hyperfine-mediated effects in a Lu^+ optical clock. *Physical Review A*, 102(5):052834, 2020.
- [17] R Kaewuam, TR Tan, Zhiqiang Zhang, KJ Arnold, MS Safronova, and MD Barrett. Precision measurement of the 3D_1 and 3D_2 quadrupole moments in Lu^+ . *Physical Review A*, 102(4):042819, 2020.
- [18] Kyle J Arnold, Rattakorn Kaewuam, Arpan Roy, T Rei Tan, and Murray D Barrett. Blackbody radiation shift assessment for a lutetium ion clock. *Nature communications*, 9(1):1–6, 2018.
- [19] KJ Arnold, R Kaewuam, TR Tan, SG Porsev, MS Safronova, and MD Barrett. Dynamic polarizability measurements with $^{176}\text{Lu}^+$. *Physical Review A*, 99(1):012510, 2019.
- [20] Till Rosenband, Piet O Schmidt, David B Hume, Wayne M Itano, Tara M Fortier, Jason E Stalnaker, K Kim, Scott A Diddams, JCJ Koelemeij, JC Bergquist, et al. Observation of the $^1S_0 \rightarrow ^3P_0$ clock transition in $^{27}\text{Al}^+$. *Physical review letters*, 98(22):220801, 2007.
- [21] J Cao, P Zhang, J Shang, K Cui, J Yuan, S Chao, S Wang, H Shu, and X Huang. A compact, transportable single-ion optical clock with 7.8×10^{-17} systematic uncertainty. *Applied Physics B*, 123(4):112, 2017.
- [22] N Huntemann, B Lipphardt, M Okhapkin, Chr Tamm, E Peik, AV Taichenachev, and VI Yudin. Generalized ramsey excitation scheme with suppressed light shift. *Phys. Rev. Lett.*, 109(21):213002, 2012.
- [23] JE Bernard, L Marmet, and AA Madej. A laser frequency lock referenced to a single trapped ion. *Optics communications*, 150(1-6):170–174, 1998.
- [24] Wayne M Itano. External-field shifts of the $^{199}\text{Hg}^+$ optical frequency standard. *Journal of research of the National Institute of Standards and Technology*, 105(6):829, 2000.
- [25] M. D. Barrett. Developing a field independent frequency reference. *New Jour. Phys.*, 17:053024, 2015.
- [26] R Kaewuam, TR Tan, KJ Arnold, SR Chanu, Zhiqiang Zhang, and MD Barrett. Hyperfine averaging by dynamic decoupling in a multi-ion lutetium clock. *Physical review letters*, 124(8):083202, 2020.
- [27] Kyle J Arnold, Rattakorn Kaewuam, Sapam R Chanu, Ting Rei Tan, Zhiqiang Zhang, and Murray D Barrett. Precision measurements of the $^{138}\text{Ba}^+ 6s \ ^2S_{1/2} - 5d \ ^2D_{5/2}$ clock transition. *Physical Review Letters*, 124(19):193001, 2020.
- [28] M Chwalla, K Kim, T Monz, P Schindler, M Riebe, CF Roos, and R Blatt. Precision spectroscopy with two correlated atoms. *Applied Physics B*, 89(4):483–488, 2007.
- [29] Chin-Wen Chou, DB Hume, Michael J Thorpe, David J Wineland, and T Rosenband. Quantum coherence between two atoms beyond $Q = 10^{15}$. *Physical review letters*, 106(16):160801, 2011.
- [30] Ethan R Clements, May E Kim, Kaifeng Cui, Aaron M Hankin, Samuel M Brewer, Jose Valencia, Jwo-Sy Chen, Chin-Wen Chou, David R Leibbrandt, and David B Hume. Lifetime-limited interrogation of two independent $^{27}\text{Al}^+$ clocks using correlation spectroscopy. *Physical Review Letters*, 125(24):243602, 2020.
- [31] VI Yudin, AV Taichenachev, CW Oates, ZW Barber, ND Lemke, AD Ludlow, U Sterr, Ch Lisdat, and F Riehle. Hyper-ramsey spectroscopy of optical clock transitions. *Physical Review A*, 82(1):011804, 2010.
- [32] DJ Berkeland, JD Miller, JC Bergquist, WM Itano, and DJ Wineland. Minimization of ion micromotion in a paul trap. *J. of Appl. Phys.*, 83(10):5025–5033, 1998.
- [33] HCJ Gan, G Maslennikov, K-W Tseng, TR Tan, R Kaewuam, KJ Arnold, D Matsukevich, and MD Barrett. Oscillating-magnetic-field effects in high-precision metrology. *Physical Review A*, 98(3):032514, 2018.
- [34] R Hobson, W Bowden, SA King, PEG Baird, IR Hill, and P Gill. Modified hyper-ramsey methods for the elimination of probe shifts in optical clocks. *Physical Review A*, 93(1):010501, 2016.
- [35] Sergei Nikolaevich Kuznetsov, Aleksei Vladimirovich Taichenachev, Valerii Ivanovich Yudin, N Hunteman, K Sanner, K Tamm, and Ekkehard Peik. Effect of trapped-ion heating on generalised ramsey methods for suppressing frequency shifts caused by a probe field in atomic clocks. *Quantum Electronics*, 49(5):429, 2019.
- [36] Samuel M Brewer, J-S Chen, Aaron M Hankin, Ethan R Clements, Chin-wen Chou, David J Wineland, David B Hume, and David R Leibbrandt. $^{27}\text{Al}^+$ quantum-logic clock with a systematic uncertainty below 10^{-18} . *Physical review letters*, 123(3):033201, 2019.
- [37] Ting Rei Tan, Rattakorn Kaewuam, Kyle J Arnold, Sapam R Chanu, Zhiqiang Zhang, MS Safronova, and Murray D Barrett. Suppressing inhomogeneous broadening in a lutetium multi-ion optical clock. *Physical review letters*, 123(6):063201, 2019.
- [38] Boulder Atomic Clock Optical Network BACON Collaboration. Frequency ratio measurements at 18-digit accuracy using an optical clock network. *Nature*, 591(7851):564–569, 2021.
- [39] Sören Dörscher, Nils Huntemann, Roman Schwarz, Richard Lange, Erik Benkler, Burghard Lipphardt, Uwe Sterr, Ekkehard Peik, and Christian Lisdat. Optical frequency ratio of a $^{171}\text{Yb}^+$ single-ion clock and a ^{87}Sr lattice clock. *Metrologia*, 58(1):015005, 2021.
- [40] Artem A Golovizin, Dmitry O Tregubov, Elena S Fedorova, Denis A Mishin, Daniil I Provorchenko, Ksenia Yu Khabarova, Vadim N Sorokin, and Nikolai N Kolachevsky. Simultaneous bicolor interrogation in thulium optical clock providing very low systematic frequency shifts. *Nature communications*, 12(1):1–9, 2021.

Supplemental Material for $^{176}\text{Lu}^+$ clock comparison at the 10^{-18} level via correlation spectroscopy

Zhang Zhiqiang,¹ K. J. Arnold,^{1,2} R. Kaewuam,¹ and M. D. Barrett^{1,3,4,*}

¹*Centre for Quantum Technologies, 3 Science Drive 2, 117543 Singapore*

²*Temasek Laboratories, National University of Singapore, 5A Engineering Drive 1, 117411 Singapore*

³*Department of Physics, National University of Singapore, 2 Science Drive 3, 117551 Singapore*

⁴*National Metrology Centre, Agency for Science, Technology and Research (A*STAR), 8 CleanTech Loop, Singapore 637145*

We provide additional information relevant to the $^{176}\text{Lu}^+$ clock comparison. A discussion of additional shifts that have been considered but do not affect the comparisons reported are given. We evaluate the sensitivity of hyperfine averaged Ramsey spectroscopy (HARS) to imperfections in timing, optical coupling, and microwave couplings. In relation to this we include a discussion of the Physikalisch-Technische Bundesanstalt (PTB) demonstration of hyper-Ramsey spectroscopy in the context of what it means for our system. We also include: expressions for evaluating the microwave ac-Zeeman systematic; a back-of-the-envelope estimate for a reasonable temperature rise for our systems; and systematic uncertainty budgets for Experiments 1 to 6.

I. ADDITIONAL CLOCK SHIFTS.

Clock shifts considered but not included in the error budget are given here. These shifts do not affect the comparisons made in this work under any realistic circumstances.

AC-Zeeman shifts: Additional ac-Zeeman shifts arise from two sources. The first concerns the ac coupling between Zeeman states. These do not cause a clock shift directly, but they do modify the effective g -factor of the level or equivalently the B-field determined by measuring a Zeeman splitting. With the rf field at the μT level, this only affects the measured field at the 10^{-9} level. At 50 Hz, we estimate field noise to be around 8 nT rms, which similarly affects the measured field at the 10^{-9} level. The second source arises from the coupling between fine-structure levels. This has both a scalar and tensor contribution, but the latter is eliminated by hyperfine averaging (HA). The former is determined by $\alpha_z \langle B^2 \rangle$ where B is the total ac-field. This has the same magnitude as the measured perpendicular component, as determined by measurements from three orthogonal directions [1]. For determination of α_z , this influences $\langle B_1^2 \rangle - \langle B_2^2 \rangle$ by $\lesssim 10^{-6}$ fractionally, compared to the 1.7×10^{-4} fractional inaccuracy of α_z . Similarly, the influence on a comparison when the clocks are both at low field is $\sim 10^{-20}$.

The blackbody radiation (BBR) shift: The polarizability for the 848-nm transition in $^{176}\text{Lu}^+$ has been very well characterized [2, 3]. The corresponding BBR shift is the lowest of any clock candidate under active investigation with an estimated shift of $-1.36(10) \times 10^{-18}$ at 300 K. For the comparison result reported we are only concerned with the frequency difference. Even allowing for one trap at 25 °C and the other at 45 °C, the contribution to the frequency difference would be just

$\sim 5 \times 10^{-19}$, and well below our measurement resolution. Given the near identical construction of the two traps and the similar trap drive powers supplied to each, such a temperature differential is highly unlikely. We also note that a temperature assessment with an inaccuracy of 2 °C has been reported [4], which was based on measurements made on a trap of identical construction, with simulations to account for different mounting within the vacuum chambers [5]. In our case the mounting is also identical. In such an assessment it must be assumed that traps of near identical construction have near identical temperatures, at least better than 2 °C in fact. Although we would not be so bold as to suggest the traps have a temperature difference of $\lesssim 2$ °C, we think it reasonable to assume the temperature difference is significantly less than 20 °C and not have any relevance to the comparisons made here. As we are unable to make a measurement of the temperature in either system and any reasonable temperature difference is immaterial to the final result, we do not include this in the comparison assessment. In addition, we give a back-of-the-envelope analysis in section IV to crudely bound the temperature and hence BBR shift for each system.

AOM Chirp: The switching of acousto-optic modulators (AOMs) and microwave sources can potentially introduce artificial frequency shifts [7] even when path lengths are nominally stabilized. Following the methodology reported in Ref.[8], this was investigated in preliminary experiments and estimated to be below 10^{-19} for the experiments reported here.

Probe induced ac-Stark shift: For the final comparison, which includes a hyper-Ramsey pulse, we have omitted any contribution from the probe-induced ac-Stark shift. Similar to experiment 7, the probe-induced ac-Stark shift was approximately 7 Hz during the pulses with a differential between the two-systems of 0.52(0.47) Hz. As evidenced by experiment 7, the effect on the comparison is already at the level of the measurement precision, even without the hyper-Ramsey pulse. Conse-

* phybmd@nus.edu.sg

quently, any level of suppression would be beyond our measurement precision. As shown in section II, for small microwave detunings, the shift has the same cubic dependence on the effective ac-Stark shift with only minor modifications from the microwave detunings. Hence, even if the frequency was not shifted during the optical pulses, the shift would only influence the comparison at the mid 10^{-19} level. As the net effective shift is trivially stable at the 0.5 Hz level, the shift of each system will be limited by the microwave coupling accuracy, which is already accounted for in the error budgets.

Timing accuracy: For HARS, timing accuracy of the pulse sequence can influence the dwell time in each state, which could potentially degrade the averaging. If the dwell time for each F is $T + \tau_1 + \tau_2 + \delta T_F$, then, using Eq. 7 from Ref[6], the clock shift δ will be

$$\delta = \frac{1}{T_R} \sum_F \Delta_F \delta T_F = \frac{\Delta_2 \delta T_6 - \Delta_1 \delta T_8}{T_R}$$

where Δ_F are linear combinations of the microwave detunings Δ_1, Δ_2 as defined in Ref[6]. For the second equality we have used the fact that $\langle \delta T_F \rangle = 0$ as any non-zero value can be absorbed in the definition of T . The on-board 100 MHz clocks of the digital I/O boards are externally synchronized so the main considerations are switching delays of clock laser AOM's and microwave sources. Switching delays of the clock laser AOM's are ~ 60 ns. However, as this doesn't influence the overall dwell time in $|8\rangle$, it doesn't result in a clock shift. Switching time differences of microwave sources only influence the synchronization at the 5 ns level. Hence, for the Hertz level detunings of the microwave fields, fractional shifts are well below 10^{-21} for all experiments reported here.

Imperfections in the implementation of HARS: As noted in the main text, microwave detunings, the finite duration of the optical pulses, and imperfect coupling strengths of the microwave and optical fields can compromise the effectiveness of our interrogation technique. A detailed analysis of these effects are provided in section II, but we summarize the main findings here. The leading order effect is due to the finite duration of the optical pulses, which is associated with an effective time $2\tau_L/\pi$ spent in $|8\rangle$. When not accounted for, it results in an effective timing error given by Eq. S3. An additional error given by Eq. S17 has the same form, which arises from deviations of the optical coupling Ω_L from the ideal condition $\Omega_L \tau_L = \pi$. From the analysis following Eq. S19, both of these corrections are practically eliminated when including a hyper-Ramsey pulse. As seen in Eq. S13, there is an additional term that is practically independent of τ_L , and this term is very well approximated by the analytic expression given in Eq. S15, which is an oscillatory function with an amplitude that is quadratic in the microwave detunings normalized by the coupling strengths. For the microwave detunings used here, this term has no significant contribution to the analysis and

is only slightly modified when including a hyper-Ramsey pulse. However, a contribution from this term arises from imperfect microwave couplings as discussed in relation to Eq. S18. As illustrated in Fig. 5 and Fig. 6 of the supplemental, the effect is to add a constant to the quadratic amplitude, and we use this amplitude to bound the contribution as an uncertainty.

Microwave detunings used in this work were measured and set with a resolution of approximately 0.1 Hz. However, at the larger operating field of 1.9 mT, variations in the magnetic field could change the detunings by up to ± 2 Hz. Data analysis has included these variations using the corrections provided by Eq. S3. As a consistency check, Eq. S16 was also used to confirm that it gave no statistically significant difference in the final results.

Uncertainty in α_z : Complete measurement results and uncertainty budgets for experiments 1-6 are given in section V. The leading systematic is due to the ac-Stark shift, which is uncorrelated as it is remeasured between experiments. For this reason the statistical and ac-Stark uncertainties are summed in quadrature and only these used to evaluate the weighted mean value $\alpha_z = -4.89264(81)$ with $\chi_\nu = 1.3$. The HARS timing systematic is correlated across experiments as all microwave detunings are dependent on just a few parameters via (S3) and (S4). These parameters are randomly resampled within their stated uncertainties to find the additional variance in the weighted mean α_z . The standard deviation is added in quadrature to the uncertainty in α_z above to arrive at $-4.89264(88)$. All other systematics are generally correlated across experiments but do not contribute significantly to the uncertainty.

II. HARS SENSITIVITY FACTORS

The Hamiltonian governing hyperfine averaged Ramsey spectroscopy (HARS) is given by [6]

$$H = \delta |g\rangle \langle g| - \sum_F \Delta_F |F\rangle \langle F| + \frac{\Omega_L}{2} (|\bar{F}\rangle \langle g| + |g\rangle \langle \bar{F}|) + \frac{\Omega_2}{2} (|6\rangle \langle 7| + |7\rangle \langle 6|) + \frac{\Omega_1}{2} (|7\rangle \langle 8| + |8\rangle \langle 7|). \quad (\text{S1})$$

where detunings

$$\Delta_6 = \frac{2\Delta_2 + \Delta_1}{3}, \quad \Delta_7 = -\frac{\Delta_2 - \Delta_1}{3}, \quad (\text{S2a})$$

and

$$\Delta_8 = -\frac{2\Delta_1 + \Delta_2}{3}, \quad (\text{S2b})$$

are linear combinations of the microwave detunings Δ_1 and Δ_2 from the $|8\rangle \leftrightarrow |7\rangle$ and $|7\rangle \leftrightarrow |6\rangle$ transitions respectively.

In [6] we demonstrated the use of this technique in reducing inhomogeneous broadening. However the result

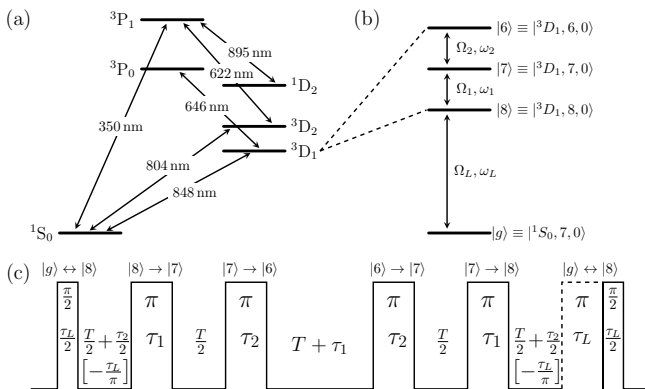


FIG. 1. Timing sequence followed for the simulations presented here. The additional π pulse (dashed) is optionally included for hyper-Ramsey spectroscopy. Reduction of the dwell time in $|8\rangle$ by $\frac{2\tau_L}{\pi}$ (terms in square brackets) can compensate for the time spent in $|8\rangle$ during the optical $\pi/2$ pulses when not using hyper-Ramsey.

was derived in the limit of small detunings and neglected the finite duration of the enclosing optical Ramsey pulses. Given the levels of accuracy we are now achieving it is pertinent to reconsider those limits. Here we simulate the full equations to illustrate the effects of operating outside these limitations and compare with analytic calculations. We use the timing sequence shown in Fig. 1 which was used in our recent comparison work as a case study. Although the frequency shifts can be numerically calculated for a given set of parameters, we provide a number of analytic approximations that accurately determine the shifts and illustrate how they are influenced by the various experimental parameters. Consequently it is sufficient to take $\tau_1 = \tau_2 = \tau = 24$ ms, $T = 0.2$ s, and $\tau_L = 8$ ms as default values for the purpose of illustration.

The main limitation that the optical π -time τ_L imposes is that it does not account for the effective time spent in the upper state during the pulse. This can be accounted for by reducing the dwell time in $|\bar{F}\rangle = |8\rangle$ by $2\tau_L/\pi$, which we henceforth refer to as the compensated sequence. The $2/\pi$ scale factor can be understood in the context of the sensitivity factor introduced in [9]. As this can be considered a timing error, we expect a frequency error given by

$$\delta = -\frac{\frac{2}{\pi}\tau_L}{3(T + 2\tau) + \frac{2}{\pi}\tau_L} \Delta_8, \quad (\text{S3})$$

which is easily derived from the considerations given in [6]. However, this does not take into account any further deviations arising from the microwave detunings. To illustrate this, we plot the actual shift as a function of Δ_1 in Fig. 2, both with and without the compensation time, and the linear approximation given by Eq. (S3). As seen in the figure, the linear approximation captures the overall trend but there are further corrections that should be considered at our current level of accuracy. In addition,

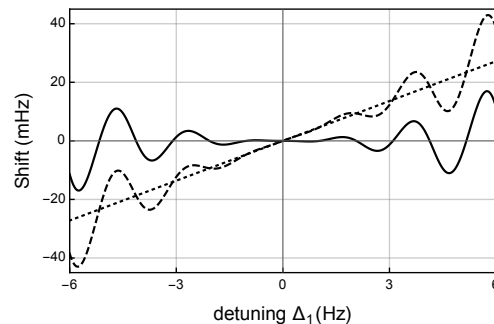


FIG. 2. Shift in the clock frequency as a function of the microwave detuning Δ_1 with (solid line) and without (dashed) compensating for the optical π -time. The dotted straight line is the linear approximation given by Eq. (S3). Parameters are given by $\tau_1 = \tau_2 = \tau = 24$ ms, $T = 0.2$ s, and $\tau_L = 8$ ms.

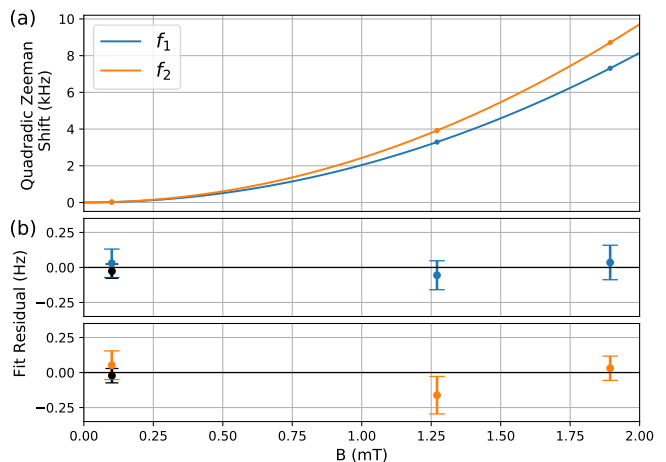


FIG. 3. Calibration of the resonant microwave frequencies. (a) Each point is the weighted mean of all measurements in Lu-1 at the three operating magnetic fields. Solid lines are the quadratic fit. Frequencies are plotted as the shift relative to $f_{1,0}$ ($f_{2,0}$) (b) Residuals of the points with respect to the fit. Black points are the measurements in Lu-2.

it is also pertinent to consider the effect of imperfect coupling strengths of both the microwave and optical fields, which can also influence the accuracy achievable by the interrogation technique.

The resonant microwave frequencies f_1 and f_2 were measured at several points between experiments when resetting the microwave detunings Δ_k near zero. These were measured using Ramsey spectroscopy with between 50 ms and 200 ms interrogation times and had typical uncertainty of ≈ 0.1 Hz per measurement. From multiple measurements in Lu-1 at $B = (0.1, 1.2, \text{ and } 1.9)$ mT, we fit to the model

$$f_1 = f_{1,0} + \alpha_{78} B^2 \quad (\text{S4})$$

$$f_2 = f_{2,0} + \alpha_{67} B^2 \quad (\text{S5})$$

as shown in Fig. 3 and find parameters

$$\begin{aligned} f_{1,0} &= 10\,491\,519\,945.035(92) \text{ Hz} \\ f_{2,0} &= 11\,290\,004\,290.255(95) \text{ Hz} \\ \alpha_{78} &= 2\,038.533(44) \text{ Hz/mT}^2 \\ \alpha_{67} &= 2\,428.945(37) \text{ Hz/mT}^2. \end{aligned}$$

Lu-2 was only operated at 0.1 mT but microwave measurements are in agreement with this model.

The magnetic field was determined with a projection-noise-limited uncertainty of ≈ 20 nT per measurement by measuring the Zeeman splitting between $|6, \pm 1\rangle$ and using the previously determined g -factors [10]. Measurements were interleaved with each clock interrogation and the field was observed to drift by no more than ± 200 nT throughout the course of any experiment. During each experiment the microwave drive frequencies ω_k were fixed and the detunings Δ_k were evaluated in later analysis from the interleaved magnetic field measurements and Eqs. (S4,S5). For all experiment $|\Delta_k| < 2$ Hz. The uncertainties in the average Δ_k for each experiment, and thus the resulting HARS timing error systematic, are limited by the precision of f_k from Eqs. (S4,S5).

Coupling strengths, or equivalently the π -times, for both microwave and optical transitions were determined from Rabi flopping curves on the respective transition, with a typical uncertainty $\sim 1\%$. Drifts in the optical coupling can be bounded to $\pm 2.5\%$ from the stability of repeated measurements of the ac-Stark shift. For the microwave couplings, repeated measurements throughout the measurement campaign indicate a $\pm 1.0\%$ stability.

To derive an expression for the error we first note that an error signal is derived from the HARS sequence by measuring the population difference between two sequences in which the last pulse is phase shifted by $\pm\pi/2$. The frequency error is then determined by the detuning δ for which

$$|c_+|^2 - |c_-|^2 = 4 \text{Re}(c_1 c_2^*) = 0 \quad (\text{S6})$$

where c_{\pm} are the final population amplitudes for the sequence with a corresponding phase shift of $\pm\pi/2$ and $c_{\pm} = c_1 \pm c_2$ are introduced for convenience. Deriving expressions for c_1 and c_2 is facilitated by expressing the operators for the various pulses in terms of the functions

$$f(x, y, a) = \cos\left(a\sqrt{x^2 + y^2}\right) + i \frac{y}{\sqrt{x^2 + y^2}} \sin\left(a\sqrt{x^2 + y^2}\right), \quad (\text{S7})$$

and

$$g(x, y, a) = \frac{x}{\sqrt{x^2 + y^2}} \sin\left(a\sqrt{x^2 + y^2}\right).$$

Equations for the frequency error for both the compensated and uncompensated sequences are almost identical and may be written

$$\text{Re}\{ie^{i\theta} F(\bar{\Omega}_L, X) G(\bar{\Omega}_1, \bar{\Omega}_2, \bar{\Delta}_1, \bar{\Delta}_2)\} = 0$$

where

$$F(\bar{\Omega}_L, X) = 4f^2(\bar{\Omega}_L, X, \frac{\pi}{4})g^2(\bar{\Omega}_L, X, \frac{\pi}{4})e^{-2iX} \quad (\text{S8})$$

and

$$\begin{aligned} G(\bar{\Omega}_1, \bar{\Omega}_2, \bar{\Delta}_1, \bar{\Delta}_2) &= f^2(\bar{\Omega}_1, -\bar{\Delta}_1, \frac{\pi}{2}) e^{i\pi\bar{\Delta}_1/2} e^{-i\phi_1} \\ &\quad - g^2(\bar{\Omega}_1, \bar{\Delta}_1, \frac{\pi}{2}) f^2(\bar{\Omega}_2, -\bar{\Delta}_2, \frac{\pi}{2}) e^{i\pi\bar{\Delta}_2/2} e^{-i\phi_2} + g^2(\bar{\Omega}_1, \bar{\Delta}_1, \frac{\pi}{2}) g^2(\bar{\Omega}_2, \bar{\Delta}_2, \frac{\pi}{2}). \end{aligned} \quad (\text{S9})$$

In the above expressions

$$\bar{\Omega}_k = \Omega_k \tau / \pi, \quad \bar{\Omega}_L = \Omega_L \tau_L / \pi, \quad \bar{\Delta}_k = \Delta_k \tau / \pi,$$

$$X = (\delta + \Delta_8) \tau_L / \pi,$$

$$\phi_1 = (T + 2\tau)(2\Delta_1 + \Delta_2) - \Delta_1 \tau / 2,$$

and

$$\phi_2 = (T + \frac{3}{2}\tau) \Delta_2.$$

The only difference in the equations, for the compensated and uncompensated case is in the parameter θ , which is given by

$$\theta = \delta [3(T + 2\tau)] = \delta T_R, \quad (\text{S10})$$

in the compensated case or

$$\begin{aligned} \theta &= \delta [3(T + 2\tau) + 2\tau_L / \pi] + 2\Delta_8 \tau_L / \pi, \\ &= \delta T_R + \frac{2\tau_L}{\pi} \Delta_8, \end{aligned} \quad (\text{S11})$$

in the uncompensated case. In both cases T_R is the effective Ramsey time for the sequence, which differs only by the compensation time $2\tau_L / \pi$.

Solution to Eq.(S6) is best understood by first considering the case in which $\bar{\Omega}_L = \bar{\Omega}_k = 1$ and using the approximation $F(1, X) \approx 1$. In a series expansion of $F(1, X)$, odd and even terms are purely imaginary and real respectively, with the next non-zero order being $\approx 0.1iX^3$. Consequently the approximation is exceptionally good under practical operating conditions and leads

to the expression

$$\text{Re} \{ i e^{i\theta} G(\bar{\Delta}_1, \bar{\Delta}_2) \} = 0 \quad (\text{S12})$$

where we have dropped the parameters $\bar{\Omega}_k$ for notational convenience. Thus,

$$\delta = -\frac{2}{\pi} \frac{\tau_L}{T_R} \Delta_8 - \frac{1}{T_R} \tan^{-1} \left(\frac{\text{Im} [G(\bar{\Delta}_1, \bar{\Delta}_2)]}{\text{Re} [G(\bar{\Delta}_1, \bar{\Delta}_2)]} \right), \quad (\text{S13})$$

where the first term only applies for the uncompensated case and is exactly the timing error given in Eq. (S3). The second term is common to both and only differs in the definition of T_R , which has the only dependence on τ_L for the second term. This illustrates the separation of the error into a timing error associated with the uncompensated finite time of the optical pulse and that associated with the microwave detunings.

A further simplification makes use of the approximation

$$f^2(1, -x, \frac{\pi}{2}) e^{i\pi x/2} \approx -x^2. \quad (\text{S14})$$

As is the case for $F(1, X)$, odd and even terms in the series expansion are purely imaginary and real respectively. Moreover, the third order term vanishes. Thus the imaginary component only appears at fifth order in x . As $g^2(1, x, \pi/2)$ is strictly real and even, the same conclusion applies to the second term in Eq. S9. This leads to the approximation

$$\delta = -\frac{2}{\pi} \frac{\tau_L}{T_R} \Delta_8 + \frac{\bar{\Delta}_2^2 \sin(\phi_2) - \bar{\Delta}_1^2 \sin(\phi_1)}{T_R}, \quad (\text{S15})$$

which also utilizes the approximation $\tan^{-1} x \approx x$ consistent with the second order expansion given in Eq. (S14). This expression accurately captures the oscillatory behaviour of the correction relative to Eq. S3 and its dependence on Δ_k , τ and T .

The quality of the approximations given in Eq. (S13) and Eq. (S15) is illustrated in Fig. 4, which shows the difference in the estimated clock shift between the value found numerically without any approximations and those found using Eq. (S15) (black) and Eq. (S13) (blue) with the latter increased by a factor of 100 to better demonstrate the dependence on detuning. Over the practical range of ± 2 Hz the approximation from Eq. (S15) is better than 5×10^{-20} of the optical frequency and Eq. (S13) is practically exact. For the parameters chosen, the ± 2 Hz corresponds to about 10% of the microwave Rabi frequency.

The effect of non-ideal couplings for the optical and microwave fields can be determined by setting $\bar{\Omega}_L = 1 + q$ and $\bar{\Omega}_k = 1 + q_k$ and including q and q_k in the relevant expansion. For the optical field it can be shown that

$$F(1 + q, X) \approx \cos^2 \left(\frac{\pi}{2} q \right) e^{2ih(q)X} + \mathcal{O}(qX^2) \quad (\text{S16})$$

where

$$\begin{aligned} h(q) &= \frac{1}{1+q} \tan \left(\frac{\pi}{2} q \right) + \frac{1}{1+q} \sec \left(\frac{\pi}{2} q \right) - 1 \\ &\approx \left(\frac{\pi}{2} - 1 \right) q. \end{aligned}$$

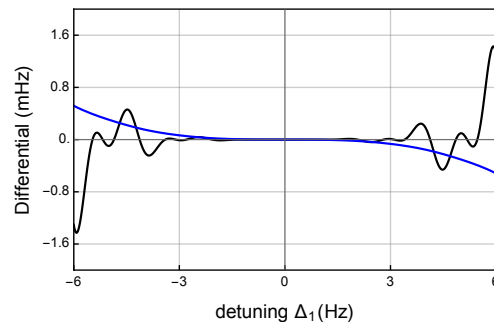


FIG. 4. Plots show the difference in the estimated clock shift between the value found numerically without any approximations and those found using Eq. (S15) (black) and Eq. (S13) (blue) with the latter increased by a factor of 100 to better highlight the dependence on detuning. Parameters are as for Fig. 2.

The amplitude factor has no influence on the resulting equation for θ but the phase factor results in an effective timing error

$$-\frac{2}{\pi} \frac{\tau_L}{T_R} \Delta_8 h(q) \approx -\frac{2}{\pi} \frac{\tau_L}{T_R} \Delta_8 \left(\frac{\pi}{2} - 1 \right) q \quad (\text{S17})$$

and will be present in either the compensated or uncompensated case. For the experiments reported here this would be $\sim 10^{-17}q$. For $q < 0.1$, this is $\lesssim 10^{-18}$, so this effect would not have a significant effect on any results stated in the report. Furthermore, as the ac-Stark shift was measured at several points over the course the measurements, we can conclude that the coupling Ω_L was stable to at least the $\sim 2.5\%$ level. Moreover, we would expect any variations to average down, so any bias of a measurement would arise from the initial assessment of the π -time which effectively determines Ω_L . We would expect it to be as probable for the π -time to be overestimated as it is to be underestimated and hence this should not bias the average over multiple measurements. Hence this effect would not affect our results at the level of precision claimed.

For the microwave fields, we follow a similar procedure. Writing $\bar{\Omega}_1 = 1 + q_1$, we obtain the second order expansion

$$f^2(1 + q_1, -x, \frac{\pi}{2}) e^{i\pi x/2} \approx -(x - i\frac{\pi}{2}q_1)^2,$$

and this also applies when including the additional g^2 function that appears in the second term of Eq. S9. The effect of imperfect coupling then is to modify the phases ϕ_k in Eq. S15 and replace the amplitudes $\bar{\Delta}_k^2$ by $\bar{\Delta}_k^2 + (\pi q_k/2)^2$. Hence the quadratic envelope of the oscillations is now offset by $(\pi q_k/2)^2$ as illustrated in Fig. 5. For $\bar{\Delta}_k \ll 1$, the modified error curve can be approxi-

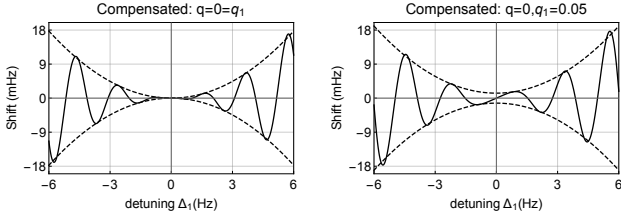


FIG. 5. Shift in the clock frequency as a function of the microwave detuning Δ_1 compensated for the optical π -time. Plot on the left assumes ideal microwave and optical couplings and the dashed lines show the expected quadratic envelope as determined by Eq. S15. Plot on the right has the microwave coupling Ω_1 increased by 5% ($q_1 = 0.05$) and the dashed lines are the offset quadratic envelope as discussed in the text. Parameters for both are as for Fig. 2.

mated by adding

$$\delta_m = \frac{\left(\bar{\Delta}_2^2 - \left(\frac{\pi q_2}{2}\right)^2\right) \sin \phi_2 + \pi \bar{\Delta}_2 q_2 \cos \phi_2}{T_R} - \frac{\left(\bar{\Delta}_1^2 - \left(\frac{\pi q_1}{2}\right)^2\right) \sin \phi_1 + \pi \bar{\Delta}_1 q_1 \cos \phi_1}{T_R}, \quad (\text{S18})$$

to Eq. S15.

An analytic result for the inclusion of a hyper-Ramsey pulse is significantly more tedious, but the same procedure can be followed. This leads to a similar equation with the form

$$\text{Re} \left\{ i e^{i\theta} \bar{F}(X) G(\bar{\Delta}_1, \bar{\Delta}_2) + \bar{H}(X, \bar{\Delta}_1, \bar{\Delta}_2) \right\} = 0, \quad (\text{S19})$$

where we have omitted the dependence on coupling strengths for notational convenience noting that a dependence on X or $\bar{\Delta}_k$ has an implied dependence on $\bar{\Omega}_L$ or $\bar{\Omega}_k$, respectively. The function G is as given in Eq. S9, and θ is as given in Eq. S10 for the compensated case. Writing the coupling strengths in the form

$$\bar{\Omega}_L = 1 + q, \quad \bar{\Omega}_k = 1 + q_k,$$

it can be shown that

$$\bar{F}(X) \approx e^{-i\pi q X}, \quad (\text{S20})$$

similar to $F(X)$, and

$$\begin{aligned} \bar{H}(X, \bar{\Delta}_1, \bar{\Delta}_2) &\approx -\pi q (X - i\frac{\pi}{2} q) \\ &- 2X \left[\left(\bar{\Delta}_1^2 + \left(\frac{\pi q_1}{2} \right)^2 + \left(\bar{\Delta}_1 - i\frac{\pi q_1}{2} \right)^2 e^{-i\phi_1} \right) \right. \\ &\left. + \left(\bar{\Delta}_2^2 + \left(\frac{\pi q_2}{2} \right)^2 - \left(\bar{\Delta}_2 - i\frac{\pi q_2}{2} \right)^2 e^{-i\phi_2} \right) \right]. \end{aligned} \quad (\text{S21})$$

Hence to lowest order, we have the same result as for the compensated sequence. That is, the hyper-Ramsey pulse suppresses the shift from the uncompensated optical pulse duration. The main difference between the

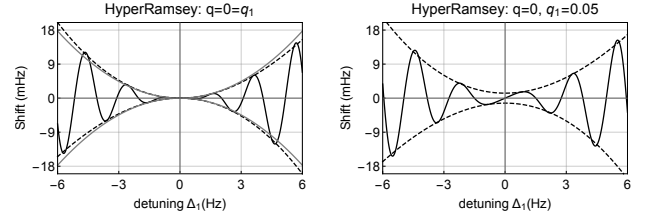


FIG. 6. Shift in the clock frequency as a function of the microwave detuning Δ_1 for the hyper-Ramsey sequence. Plot on the left assumes ideal microwave and optical couplings and the dashed lines show the expected quadratic envelope modified by the additional term in Eq. S19. For comparison, the gray lines give the quadratic envelope for the compensated sequence. Plot on the right has the microwave coupling Ω_1 increased by 5% ($q_1 = 0.05$) and the dashed lines are the offset envelope as discussed in the text. Parameters for both are as for Fig. 2.

hyper-Ramsey sequence and compensated case comes from the additional \bar{H} term which, to a good approximation, gives an additional shift.

For the dependence on the optical coupling, only the first term in Eq. S21 has a dependence on q and only the real part $-\pi q X$ contributes. This gives a shift that is equal and opposite to that arising from $\bar{F}(X) \approx e^{-i\pi q X}$ and thus cancels. Moreover, the cancellation also applies to terms of order $q^2 X$ that have been omitted. Subsequently, the shift for the hyper-Ramsey sequence is much more insensitive to imperfect optical coupling strengths than the compensated sequence.

For $q_1 = q_2 = 0$, the real part of the remaining terms can be written

$$-4X \left[\bar{\Delta}_1^2 \cos^2 \left(\frac{1}{2} \phi_1 \right) + \bar{\Delta}_2^2 \sin^2 \left(\frac{1}{2} \phi_2 \right) \right].$$

With $X \approx \Delta_8 \tau_L / \pi$, this provides a slight asymmetry to the magnitude of the shift as a function of detuning compared to the compensated case and this is illustrated in Fig. 6. In determining the modification to the envelope, it should be noted that maximum and minimum of the compensated case occur when $\sin \phi_k \approx \pm 1$. At these points $\cos^2(\phi_k/2) \approx \sin^2(\phi_k/2) \approx 1/2$.

As in the compensated case, non-zero values of q_k will offset ϕ_k appearing in the above equation and replace the amplitudes $\bar{\Delta}_k^2$ by $\bar{\Delta}_k^2 + (\pi q_k/2)^2$. However the influence of this term will be dominated by the same influence q_k has on $G(\bar{\Delta}_1, \bar{\Delta}_2)$ and this is the same for both the compensated and hyper-Ramsey cases.

We have not explicitly included the ac-Stark shift in the hyper-Ramsey case. To include this in Eq. S19, one simply makes the replacement

$$X \rightarrow (\delta - \Delta + \Delta_8) \tau_L / \pi \approx (-\Delta + \Delta_8) \tau_L / \pi,$$

where Δ is the effective frequency shift as given in Ref. [11], that is, the ac-Stark shift minus the compensating frequency step made during the optical pulses. Here there is an additional term Δ_8 . Hence the total shift is

given approximately by

$$\delta = \frac{1}{T_R} \left(\frac{4 + \pi}{2} \right) \left(\frac{(\Delta - \Delta_8)\tau_L}{\pi} \right)^3 + \delta_0$$

where δ_0 is the shift as previously discussed in the absence of Δ . When the microwave detunings Δ_k are zero, the result is exactly that obtained in Ref. [11] noting that $\Omega_L = \pi/\tau_L$. However the factor $(4 + \pi)/2$ given here is exact, where as it is specified to be approximately π in Ref. [11]. Since the two treatments are algebraically equivalent when the microwave detunings are zero, we assume the value given in Ref. [11] to be a crude approximation.

A. Measuring the level of suppression

It is worthwhile discussing what level of suppression can realistically be experimentally determined in light of the theoretical description. This has been explored by Physikalisch-Technische Bundesanstalt (PTB) and reported in [12], but the results are often misinterpreted as demonstrating orders of magnitude suppression. This comes from statements in the paper in reference to [12, Fig. 4b]. The statement made in the paper references the inset of the figure and notes that: if the effective light shift is kept within 0.5 Hz, the resulting clock shift would be well-below 10^{-17} , which represents a suppression of the shift by 4 orders of magnitude. This comment is in reference to the shift Δ_L during the Ramsey pulses, that is, it compares what is effectively an uncertainty for HRS to a full shift during the optical pulses for Ramsey spectroscopy (RS). A fair comparison should compare the uncertainties for both cases, that is, to compare RS to HRS at the same value of Δ , which amounts to a factor of 82. Furthermore, to justify this claim, the inset would need to include data that would demonstrate the cubic dependence with sufficient accuracy and that would require measurements with a precision of at least 10% of the vertical axis on the inset i.e. 2×10^{-18} , which is 170 times smaller than the uncertainties given in their figure.

The data given is completely consistent with a straight line, which the reader can readily verify. A by-eye fit with a slope of 0.125 and no offset is certainly reasonable given that no data point is more than an uncertainty away from the line (hence the reduced- χ^2 is definitely less than 1). The measurements are equally spaced by 1 Hz with an uncertainty that is approximately equal for all points at 0.25 Hz. Consequently any fitted straight line ($y = mx$) would have an uncertainty in the slope of 0.038. Hence we would estimate a slope of $m = 0.125(38)$ from the figure they present. Since the π -time for the experiment was 72 ms and the interrogation time was 144 ms, the time between the two Ramsey $\pi/2$ pulses was 216 ms. Thus conventional Ramsey spectroscopy in which the hyper-

Ramsey pulse is inactive would have a slope of

$$m = \frac{1}{1 + \frac{\pi}{2} \frac{216}{72}} = 0.175$$

This is within 1.3 standard deviations of the $m = 0.125(38)$ slope we estimate from the figure. Compared to the 0.175, this would be routinely considered consistent or even excellent agreement in the scientific literature. To be absolutely clear, the data presented is completely consistent with the hyper-Ramsey pulse being inadvertently omitted (but the duration still present). This cannot seriously be suggested as a valid demonstration of a 4-order-of-magnitude suppression or an indication of any level of validity for that matter. Note that the Stark shift was 60 Hz and the 0.5 Hz requirement represents $< 1\%$ stability requirement for the laser intensity.

For our experiment 8, the ac-Stark shift during the optical pulses is 7 Hz, the interrogation time 744 ms, and the optical π -time 8 ms. In this case, the plot corresponding to [12, Fig. 4b], would have a vertical range of ± 0.4 mHz or $\pm 1.1 \times 10^{-18}$ fractionally for the ± 5 Hz range on the horizontal axis, which is a 1000-fold smaller than for the PTB case. For the inset, the vertical range would be reduced to $\pm 8.8 \times 10^{-21}$ for the ± 1 Hz range shown. Hence properly validating suppression is well beyond our measurement capability. This general conclusion doesn't change for different parameter settings unless one considers extreme detunings comparable to the resolution of the optical pulses. We also note that the 0.5 Hz requirement for us is a trivially obtainable 7% stability of the laser intensity and reduces the shift to $\pm 1.1 \times 10^{-21}$. However this would be compromised by experimental imperfections as discussed in the previous section, which is explicitly accounted for in our error budgets.

The best that can be done is to demonstrate a high accuracy comparison and account for deviations of the experiment from ideal parameters. That is exactly what we have done and completely consistent with what PTB has done [4, 13].

III. MICROWAVE AC-ZEEMAN SHIFT

The shift from microwave ac-Zeeman shifts are given by

$$\delta = \frac{(\Delta_{1,7} + \Delta_{1,8})\tau_1 + (\Delta_{2,6} + \Delta_{2,7})\tau_2}{3(T + \tau_1 + \tau_2)}, \quad (\text{S22})$$

where $\Delta_{k,F}$ is the shift of $|F\rangle$ when Ω_k is on. Denoting the polarizations of the fields as a_{kq} and the Zeeman

splitting in each hyperfine level as $\omega_F > 0$, we have

$$\begin{aligned}\Delta_{1,8} &= -\frac{\Omega_{8,0,7,1}^2}{4\omega_7} + \frac{\Omega_{8,0,7,-1}^2}{4\omega_7}, \\ &= -\frac{7}{16} \frac{\Omega_{8,0,7,0}^2}{4\omega_7} \left[\left(\frac{a_{1+}}{a_{10}} \right)^2 - \left(\frac{a_{1-}}{a_{10}} \right)^2 \right], \\ \Delta_{1,7} &= \frac{\Omega_{8,-1,7,0}^2}{4\omega_8} - \frac{\Omega_{8,1,7,0}^2}{4\omega_8}, \\ &= \frac{9}{16} \frac{\Omega_{8,0,7,0}^2}{4\omega_8} \left[\left(\frac{a_{1+}}{a_{10}} \right)^2 - \left(\frac{a_{1-}}{a_{10}} \right)^2 \right], \\ \Delta_{2,7} &= \frac{\Omega_{7,0,6,1}^2}{4\omega_6} - \frac{\Omega_{7,0,6,-1}^2}{4\omega_6}, \\ &= \frac{3}{7} \frac{\Omega_{7,0,6,0}^2}{4\omega_6} \left[\left(\frac{a_{2+}}{a_{20}} \right)^2 - \left(\frac{a_{2-}}{a_{20}} \right)^2 \right], \\ \Delta_{2,6} &= \frac{\Omega_{7,-1,6,0}^2}{4\omega_7} - \frac{\Omega_{7,1,6,0}^2}{4\omega_7}, \\ &= \frac{4}{7} \frac{\Omega_{7,0,6,0}^2}{4\omega_7} \left[\left(\frac{a_{2+}}{a_{20}} \right)^2 - \left(\frac{a_{2-}}{a_{20}} \right)^2 \right].\end{aligned}$$

We measure the polarization ratios at a fixed (high) power and the ratio of π times is determines the ratio of the polarization components. Hence

$$\frac{a_{1\pm}}{a_{10}} = \frac{4}{3} \frac{\tau_{10}}{\tau_{1\pm}}, \quad \frac{a_{2\pm}}{a_{20}} = \sqrt{\frac{7}{3}} \frac{\tau_{20}}{\tau_{2\pm}},$$

where τ_{kq} is the π -time for the polarization q of field k and we have omitted signs from Clebsch-Gordan factors. Thus we have

$$\begin{aligned}\Delta_{1,8} + \Delta_{1,7} &= \left(-\frac{7}{9} \frac{\Omega_{8,0,7,0}^2}{4\omega_7} + \frac{\Omega_{8,0,7,0}^2}{4\omega_8} \right) Y_1, \\ \Delta_{2,7} + \Delta_{2,6} &= \left(\frac{\Omega_{7,0,6,0}^2}{4\omega_6} + \frac{4}{3} \frac{\Omega_{7,0,6,0}^2}{4\omega_7} \right) Y_2.\end{aligned}$$

where

$$Y_k = \left(\frac{\tau_{k0}}{\tau_{k+}} \right)^2 - \left(\frac{\tau_{k0}}{\tau_{k-}} \right)^2.$$

The total error is dominated by $\Delta_{1,8}$ and $\Delta_{2,6}$ due to the smaller size of the Zeeman splitting ω_7 . The factors in parentheses are given by the microwave π times and the magnetic field used in the experiment. For a π -time of $\tau_r = 1$ ms and a magnetic field of $B_r = 0.1$ mT, we have

$$\begin{aligned}a_{1r} &= \frac{1}{2\pi f_c} \left(-\frac{7}{9} \frac{\Omega_{8,0,7,0}^2}{4\omega_7} + \frac{\Omega_{8,0,7,0}^2}{4\omega_8} \right) \\ &\approx -9.62 \times 10^{-15},\end{aligned}\tag{S23}$$

$$\begin{aligned}a_{2r} &= \frac{1}{2\pi f_c} \left(\frac{\Omega_{7,0,6,0}^2}{4\omega_6} + \frac{4}{3} \frac{\Omega_{7,0,6,0}^2}{4\omega_7} \right) \\ &\approx 2.18 \times 10^{-14}.\end{aligned}\tag{S24}$$

These values can then be scaled for any experiment using the specific values of τ and T_R used giving a total fractional shift of

$$\frac{\tau_r^2 B_r}{\tau T_R B} (a_{1r} Y_1 + a_{2r} Y_2).$$

Uncertainties are dominated by the determination of Y_k , as the associated π -times are measured less accurately. Taking the same fractional uncertainty β for the π -times, we have

$$\delta Y_k = \beta \sqrt{\frac{8\tau_0^4 (\tau_+^4 - \tau_+^2 \tau_-^2 + \tau_-^4)}{\tau_-^4 \tau_+^4}},$$

where we have omitted the subscript k for convenience. If we write $\tau_{\min} = \min(\tau_+, \tau_-)$ and $\tau_{\max} = \max(\tau_+, \tau_-) = \gamma \tau_{\min}$, then the above expression can be written

$$\beta \left(\frac{\tau_0}{\tau_{\min}} \right)^2 \sqrt{8 \frac{\gamma^4 - \gamma^2 + 1}{\gamma^4}}.$$

The last term lies between $\sqrt{6}$ and $\sqrt{8}$ so is within 7% of $2.64 \approx \sqrt{7}$. Although the shift is suppressed when the circular polarizations are balanced, the uncertainty is primarily determined by their suppression.

Contributions from different k would add in quadrature giving a fractional uncertainty of

$$\frac{\tau_r^2 B_r}{\tau T_R B} \sqrt{a_{1r}^2 \delta Y_1^2 + a_{2r}^2 \delta Y_2^2}.$$

We are then able to write the fractional uncertainty for LC- n as

$$\delta_n = \alpha_n \frac{\tau_r^2 B_r}{\tau T_R B}.\tag{S25}$$

From the measured π -times for the characterizations of the polarizations, α_n differs from the mean values by only $\pm 10\%$ and we have

$$\alpha_1 \approx 7.1 \times 10^{-16}, \quad \text{and} \quad \alpha_2 \approx 3.0 \times 10^{-15}.$$

The larger value for LC-2 (by about a factor of 4) is a consequence of the fact that the microwave polarizations for the $|7\rangle \leftrightarrow |6\rangle$ were approximately equal i.e. the circular components had the worst suppression, which happened to be for the largest contribution to the error. The worst case is for experiment 5 which would have an uncertainty contribution of $\sim 7 \times 10^{-19}$ for LC-2 (at low field). For experiments 7 and 8 the uncertainty is $1 \sim 2 \times 10^{-19}$.

IV. THE BBR SHIFT

Given the very low BBR shift for the $^1S_0 \leftrightarrow ^3D_1$ transition, it is possible to make a very crude estimate to bound the shift. Our traps are four rod traps with

axial end caps and all electrodes are 0.48mm diameter rods of copper-beryllium. At each end of the trap the 5 electrodes (4 rods + end cap) are fixed in place by a $4 \times 4 \times 3$ mm cube of alumina press fit into a larger copper block ($\sim 9 \times 9 \times 9$ mm). Each copper block, top and bottom is attached to a 2mm thick copper plate which would act as an effective heat spreader. One of the plates is directly bolted to a custom outer aluminium cylinder that is bolted directly to the vacuum chamber wall. The RF rods are directly clamped to a 3 mm diameter, 5cm long, rf copper feedthrough pin.

Taking the thermal conduction in the alumina spacer only over the 90 degree angle between vertical and horizontal, the thermal resistance is ~ 5 K/W. There are two rods and two alumina spacers, so taking the resistance in parallel we would have ~ 1 K/W thermal resistance. Taking the worst-case scenario of all heat conducted along the full length of one copper plate gives an added thermal resistance of 3 K/W and we estimate a further 1.5 K/W for the outer cylinder giving $\lesssim 5.5$ K/W thermal resistance from electrode to chamber wall. This neglects any radiation losses from any surface, any conduction losses from the direct RF pin connection, and the heat spreading effect of the second copper plate. The input power for our experiment is ~ 2 W. Assuming all this is dissipated in the RF electrodes gives at most a 11 K temperature rise above the lab environment, which was no less than 25°C or 298 K during these experiments. We are aware of systems in which there has been observed much larger temperature rises such as [14], but these systems have considerably larger input powers than we use.

All things considered, we think a $35(10)^\circ\text{C}$ bound on the temperature is a conservative estimate inclusive of the worst case scenario. However, we refrain from making accuracy claims on the basis of this argument. We also stress that the comparison reported concerns the temperature difference, which is highly insensitive to an overall absolute temperature. As noted in the main text, the temperature difference would need to be significantly more than 20°C to have any bearing on the result.

V. UNCERTAINTY BUDGETS FOR EXPERIMENTS 1-6

Table I gives the measured frequency differences between Lu-1 and Lu-2 for experiments 1 to 6, with statistical and systematic uncertainties given separately. Tables II-VII give the uncertainty budgets for experiments 1 to 6.

TABLE I. Measured clock frequency differences in mHz for experiments 1-7. 'Stat.' and 'Sys.' are the statistical and systematic uncertainties respectively in mHz. B_k are the average magnetic fields in Lu- k .

Expt.	Diff.	Stat.	Sys.	B_1 (mT)	B_2 (mT)
1	-17.5177	7.4	12.1	1.894286	0.101049
2	-17.5130	2.8	6.7	1.894212	0.101040
3	-17.5012	3.2	3.8	1.894030	0.101005
4	-17.5065	3.9	6.8	1.894055	0.100967
5	-17.4992	5.3	4.0	1.894009	0.100926
6	-7.8431	2.1	3.8	1.270804	0.100552

TABLE II. Uncertainty budget for Experiment 1 in which $\tau_L = 4.4$ ms, $\tau_1 = \tau_2 = 12$ ms, $T = 100$ ms, $B_1 \approx 1.9$ mT, $B_2 \approx 0.1$ mT. All values are relative to 10^{-18} of the HA frequency.

Effect	Lu-1		Lu-2		Difference	
	Shift	Unc.	Shift	Unc.	Shift	Unc.
Excess micromotion	-0.41	0.37	-0.44	0.34	0.03	0.50
Second-order Doppler (thermal)	-1.32	0.31	-0.10	0.06	-1.22	0.32
ac-Zeeman (rf)	0.54	0.01	0.15	0.01	0.39	0.01
ac-Zeeman (microwave)	-0.03	0.01	-0.22	0.60	0.19	0.60
Gravity shift	-	-	-	-	-1.31	0.15
ac-Stark shift	-485.37	24.27	-474.83	23.74	-10.54	33.95
HARS timing	9.27	2.84	0.90	0.79	8.37	2.95
Microwave coupling	0.00	0.42	0.00	0.42	0.00	0.60
Optical coupling	0.00	0.30	0.00	0.30	0.00	0.43
Residual quadruple shift	0.22	0.02	0	0.32	0.22	0.32
Total	-477.09	24.44	-474.54	23.77	-3.87	34.10

TABLE III. Uncertainty budget for Experiment 2 in which $\tau_L = 4.4$ ms, $\tau_1 = \tau_2 = 12$ ms, $T = 200$ ms, $B_1 \approx 1.9$ mT, $B_2 \approx 0.1$ mT. All values are relative to 10^{-18} of the HA frequency.

Effect	Lu-1		Lu-2		Difference	
	Shift	Unc.	Shift	Unc.	Shift	Unc.
Excess micromotion	-0.41	0.37	-0.44	0.34	0.03	0.50
Second-order Doppler (thermal)	-1.77	0.42	-0.12	0.06	-1.64	0.42
ac-Zeeman (rf)	0.54	0.01	0.15	0.01	0.39	0.01
ac-Zeeman (microwave)	-0.02	0.00	-0.12	0.33	0.10	0.33
Gravity shift	-	-	-	-	-1.31	0.15
ac-Stark shift	-268.68	13.43	-262.85	13.14	-5.83	18.79
HARS timing	12.28	1.58	0.54	0.44	11.73	1.64
Microwave coupling	0.00	0.23	0.00	0.23	0.00	0.33
Optical coupling	0.00	0.17	0.00	0.17	0.00	0.24
Residual quadruple shift	0.22	0.02	0	0.32	0.22	0.32
Total	-257.84	13.54	-262.84	13.17	3.69	18.89

TABLE IV. Uncertainty budget for Experiment 3 in which $\tau_L = 8$ ms, $\tau_1 = \tau_2 = 12$ ms, $T = 200$ ms, $B_1 \approx 1.9$ mT, $B_2 \approx 0.1$ mT. All values are relative to 10^{-18} of the HA frequency.

Effect	Lu-1		Lu-2		Difference	
	Shift	Unc.	Shift	Unc.	Shift	Unc.
Excess micromotion	-0.41	0.37	-0.44	0.34	0.03	0.50
Second-order Doppler (thermal)	-1.77	0.42	-0.12	0.06	-1.64	0.42
ac-Zeeman (rf)	0.54	0.01	0.15	0.01	0.39	0.01
ac-Zeeman (microwave)	-0.02	0.00	-0.12	0.33	0.10	0.33
Gravity shift	-	-	-	-	-1.31	0.15
ac-Stark shift	-146.48	7.32	-144.23	7.21	-2.25	10.28
HARS timing	7.13	2.86	1.31	0.80	5.82	2.97
Microwave coupling	0.00	0.23	0.00	0.23	0.00	0.33
Optical coupling	0.00	0.31	0.00	0.31	0.00	0.43
Residual quadruple shift	0.22	0.02	0	0.32	0.22	0.32
Total	-140.78	7.89	-143.45	7.29	1.37	10.74

TABLE V. Uncertainty budget for Experiment 4 in which $\tau_L = 8$ ms, $\tau_1 = \tau_2 = 12$ ms, $T = 100$ ms, $B_1 \approx 1.9$ mT, $B_2 \approx 0.1$ mT. All values are relative to 10^{-18} of the HA frequency.

Effect	Lu-1		Lu-2		Difference	
	Shift	Unc.	Shift	Unc.	Shift	Unc.
Excess micromotion	-0.41	0.37	-0.44	0.34	0.03	0.50
Second-order Doppler (thermal)	-1.32	0.31	-0.10	0.06	-1.22	0.32
ac-Zeeman (rf)	0.54	0.01	0.15	0.01	0.39	0.01
ac-Zeeman (microwave)	-0.03	0.01	-0.22	0.60	0.19	0.60
Gravity shift	-	-	-	-	-1.31	0.15
ac-Stark shift	-264.61	13.23	-260.54	13.03	-4.06	18.57
HARS timing	34.70	5.14	2.99	1.44	31.72	5.34
Microwave coupling	0.00	0.42	0.00	0.42	0.00	0.60
Optical coupling	0.00	0.55	0.00	0.55	0.00	0.78
Residual quadruple shift	0.22	0.02	0	0.32	0.22	0.32
Total	-230.90	14.22	-258.16	13.15	25.95	19.37

TABLE VI. Uncertainty budget for Experiment 5 in which $\tau_L = 8$ ms, $\tau_1 = \tau_2 = 6$ ms, $T = 200$ ms, $B_1 \approx 1.9$ mT, $B_2 \approx 0.1$ mT. All values are relative to 10^{-18} of the HA frequency.

Effect	Lu-1		Lu-2		Difference	
	Shift	Unc.	Shift	Unc.	Shift	Unc.
Excess micromotion	-0.41	0.37	-0.44	0.34	0.03	0.50
Second-order Doppler (thermal)	-1.71	0.41	-0.12	0.06	-1.59	0.41
ac-Zeeman (rf)	0.54	0.01	0.15	0.01	0.39	0.01
ac-Zeeman (microwave)	-0.03	0.01	-0.25	0.70	0.22	0.70
Gravity shift	-	-	-	-	-1.31	0.15
ac-Stark shift	-154.77	7.74	-152.39	7.62	-2.38	10.86
HARS timing	19.17	3.02	2.16	0.84	17.01	3.14
Microwave coupling	0.00	0.25	0.00	0.25	0.00	0.35
Optical coupling	0.00	0.32	0.00	0.32	0.00	0.46
Residual quadruple shift	0.22	0.02	0	0.32	0.22	0.32
Total	-137.00	8.34	-150.90	7.72	12.59	11.37

TABLE VII. Uncertainty budget for Experiment 6 in which $\tau_L = 8$ ms, $\tau_1 = \tau_2 = 12$ ms, $T = 200$ ms, $B_1 \approx 1.2$ mT, $B_2 \approx 0.1$ mT. All values are relative to 10^{-18} of the HA frequency.

Effect	Lu-1		Lu-2		Difference	
	Shift	Unc.	Shift	Unc.	Shift	Unc.
Excess micromotion	-0.41	0.37	-0.44	0.34	0.03	0.50
Second-order Doppler (thermal)	-1.77	0.42	-0.12	0.06	-1.64	0.42
ac-Zeeman (rf)	0.54	0.01	0.15	0.01	0.39	0.01
ac-Zeeman (microwave)	-0.02	0.01	-0.12	0.33	0.10	0.33
Gravity shift	-	-	-	-	-1.31	0.15
ac-Stark shift	-153.45	7.67	-140.80	7.04	-12.64	10.41
HARS timing	-6.12	1.84	5.53	0.80	-11.64	2.00
Microwave coupling	0.00	0.23	0.00	0.23	0.00	0.33
Optical coupling	0.00	0.31	0.00	0.31	0.00	0.43
Residual quadruple shift	0.22	0.02	0	0.32	0.22	0.32
Total	-161.00	7.92	-135.80	7.12	-26.50	10.65

-
- [1] R Kaewuam, TR Tan, Zhiqiang Zhang, KJ Arnold, MS Safronova, and MD Barrett. Precision measurement of the 3D_1 and 3D_2 quadrupole moments in Lu^+ . *Physical Review A*, 102(4):042819, 2020.
- [2] Kyle J Arnold, Rattakorn Kaewuam, Arpan Roy, T Rei Tan, and Murray D Barrett. Blackbody radiation shift assessment for a lutetium ion clock. *Nature communications*, 9(1):1–6, 2018.
- [3] KJ Arnold, R Kaewuam, TR Tan, SG Porsev, MS Safronova, and MD Barrett. Dynamic polarizability measurements with $^{176}\text{Lu}^+$. *Physical Review A*, 99(1):012510, 2019.
- [4] N Huntemann, C Sanner, B Lipphardt, Chr Tamm, and E Peik. Single-ion atomic clock with 3×10^{-18} systematic uncertainty. *Phys. Rev. Lett.*, 116(6):063001, 2016.
- [5] Miroslav Doležal, Petr Balling, Peter BR Nisbet-Jones, Steven A King, Jonathan M Jones, Hugh A Klein, Patrick Gill, Thomas Lindvall, Anders E Wallin, Mikko Merimaa, et al. Analysis of thermal radiation in ion traps for optical frequency standards. *Metrologia*, 52(6):842, 2015.
- [6] R Kaewuam, TR Tan, KJ Arnold, SR Chanu, Zhiqiang Zhang, and MD Barrett. Hyperfine averaging by dynamic decoupling in a multi-ion lutetium clock. *Physical review letters*, 124(8):083202, 2020.
- [7] Fei Liu, Lijuan Gu, Shangran Xie, Xiangge He, Duo Yi, Min Zhang, and Qingchang Tao. Acousto-optic modulation induced noises on heterodyne-interrogated interferometric fiber-optic sensors. *Journal of Lightwave Technology*, 36(16):3465–3471, 2018.
- [8] Stephan Falke, Mattias Misera, Uwe Sterr, and Christian Lisdat. Delivering pulsed and phase stable light to atoms of an optical clock. *Applied Physics B*, 107(2):301–311, 2012.
- [9] G John Dick. Local oscillator induced instabilities in trapped ion frequency standards. In *Proceedings of the 19th Annual Precise Time and Time Interval Systems and Applications Meeting*, pages 133–147, 1989.
- [10] Zhiqiang Zhang, K. J. Arnold, R. Kaewuam, M. S. Safronova, and M. D. Barrett. Hyperfine-mediated effects in a Lu^+ optical clock. *Phys. Rev. A*, 102:052834, Nov 2020.
- [11] VI Yudin, AV Taichenachev, CW Oates, ZW Barber, ND Lemke, AD Ludlow, U Sterr, Ch Lisdat, and F Riehle. Hyper-ramsey spectroscopy of optical clock transitions. *Physical Review A*, 82(1):011804, 2010.
- [12] N Huntemann, B Lipphardt, M Okhapkin, Chr Tamm, E Peik, AV Taichenachev, and VI Yudin. Generalized ramsey excitation scheme with suppressed light shift. *Phys. Rev. Lett.*, 109(21):213002, 2012.
- [13] Christian Sanner, Nils Huntemann, Richard Lange, Christian Tamm, Ekkehard Peik, Marianna S Safronova, and Sergey G Porsev. Optical clock comparison for lorentz symmetry testing. *Nature*, 567(7747):204–208, 2019.
- [14] Chin-wen Chou, DB Hume, JCJ Koelemeij, David J Wineland, and Till Rosenband. Frequency comparison of two high-accuracy Al^+ optical clocks. *Physical review letters*, 104(7):070802, 2010.